RSC Advances

PAPER

View Article Online
View Journal | View Issue

Cite this: *RSC Adv.*, 2026, **16**, 13021

Effects of nucleation on solvate and polymorph control – evaporative crystallization of taltirelin

Dang Le Tri Nguyen, [a] Jungsuk Kim,*[b] Kwang-Joo Kim *[a] and Joachim Ulrich[b]

Received 14th October 2025
Accepted 14th January 2026

DOI: 10.1039/d5ra07845h

rsc.li/rsc-advances

This study focuses on the selective formation of taltirelin (TTL) solvates (hydrates) and polymorphs through evaporative crystallization. Factors influencing the nucleation of TTL polymorphs in evaporative crystallization, such as evaporation rate, supersaturation, solvent, temperature, and concentration, were investigated. In the evaporative crystallization of TTL in water, only the β-form was formed at an evaporation rate below 0.412 cm^3 $(min \cdot m^2)^{-1}$, whereas a mixture of the α-form and β-form was obtained at evaporation rates of 0.44–0.71 cm^3 $(min \cdot m^2)^{-1}$. At evaporation rates of 0.74–1.99 cm^3 $(min \cdot m^2)^{-1}$, the α-form crystals were formed. Regarding the formation conditions of solvates influenced by degree of supersaturation, the β-form was obtained at supersaturation (S) < 1.68, while a mixture of the α-form and β-form appeared in the range of 1.86 < S < 3.75. The α-form was observed within the range of 2.68 < S < 8.80. The anhydrous γ-form was obtained from methanol, ethanol, 1-propanol, and isopropanol (IPA) solvents, regardless of the supersaturation in evaporative crystallization. From the plot of dimensionless supersaturation and dimensionless solubility, the α-form was obtained when the nucleation rate was $1 \times 10^{23} < B_{het} < 6 \times 10^{23}$ nuclei per m^3 s, whereas the β-form was obtained when the nucleation rate was $2 \times 10^{22} < B_{het} < 1 \times 10^{23}$ nuclei per m^3 s. Therefore, this plotting method provides important information on nucleation rates for the selective formation of polymorphs/solvates and can also be applied to predict new polymorphs/solvates.

1 Introduction

Polymorphism refers to the ability of a solid substance to exist in multiple crystal structures. On the other hand, solvates include solvent molecules in the crystal lattice and are chemically identical.[1,2] Various polymorphs or solvates of an active pharmaceutical ingredient (API) often show differences in physical properties such as density, shape, dissolution rate or solubility, which can lead to variations in bioavailability and have a significant impact on product quality, particularly in pharmaceuticals. Recent development trends highlight the critical need and importance of polymorph and solvate screening and control for APIs.[3] Since there is currently no method to predict selective polymorph or solvate formation, experimental determination is the only way to identify or rule out polymorphs and solvates.

Crystallization technology is used for the separation and purification of APIs, enabling control over key product characteristics such as particle size, shape, solvates and polymorphism.[4–6] Crystallization methods are generally classified based on how supersaturation is achieved, with cooling, antisolvent addition, and evaporation being the main techniques. The polymorph or solvate formed during the manufacturing process can vary depending on several operational parameters, such as crystallization mode, temperature, solvent, and mixing conditions within the crystallizer.[7–10] Therefore, it is necessary to conduct detailed studies on the polymorphism or solvate state of APIs under different conditions. Additionally, polymorphism or solvates are key factors in determining the physical properties of a product and an essential specification for intellectual property ownership.

In this study, we investigated the polymorphs and solvates (hydrates) of taltirelin (TTL), an active pharmaceutical ingredient used as a central nervous system activator. The chemical structure of taltirelin is as follows: (−)-*N*-[(*s*)-hexahydro-1-methyl-2,6-dioxo-4-pyrimidinyl]-L-histidyl-L-prolinamido tetrahydrate (see Fig. SI1).

Two solvates (hydrates) of TTL, α-form and β-form, are known. The β-form is primarily used in pharmaceuticals, while the α-form, being a metastable form under ambient conditions, has potential applications due to its relatively high solubility.[11,12] Therefore, selective solvate formation is required depending on the application. Over the past 20 years, several studies have been published regarding the crystallization and transformation of TTL polymorphs and solvates.[11–17] First, this compound is a peptide composed of three components (1-methyl dihydroorotic acid, L-histidine, and L-prolinamide) and

[a]*Crystallization Process & Engineering Center, Hanbat National University, Yusung 34158, Daejeon, South Korea*

[b]*Ehe. Zentrum für Ingenieurwissenschaften, Nat Fak I, Martin-Luther-Universität Halle-Wittenberg, D-06099 Halle, Germany. E-mail: kjkim@hanbat.ac.kr*

has two crystal forms (α-form and β-form). The α-form belongs to the triclinic system, space group P1, and exhibits excellent characteristics in solid–liquid separation, making it the preferred choice as a drug substance. However, it is a metastable form within a specific temperature range. The β-form belongs to the orthorhombic system, space group $P2_12_12_1$. Second, the solubility profile of the solvates demonstrates a reversible (enantiotropic) system. This means that one solvate is stable within a specific temperature and pressure range (*i.e.*, it has a lower free energy content and solubility), while the other solvate is stable at a different temperature and pressure range. Third, α-form crystals can be converted to β-form *via* solvent-mediated transformation.[11,13,15] Maruyama *et al.*[11–13] investigated the solvent effect on the behavior of polymorphs during cooling crystallization in a mixture of water and methanol (MeOH). Different solvates and polymorphs were formed depending on the methanol concentration, and it was suggested that the conversion from form α to form β is influenced by the methanol concentration in solvent-mediated transformation. Dang *et al.*[14–17] studied the nucleation mechanisms of the two TTL polymorphs using supersaturation profiles tracked by Raman spectroscopy. Polymorph transformation was detected by monitoring the Raman spectra of both polymorphs in a slurry state. They investigated the method for solvent-mediated solvate transformation of TTL from the α-form to the β-form during seeded crystallization. The kinetics of TTL solvate transformation were revealed by the three-dimensional growth mechanism of nucleation, as described by the Avrami–Erofeev equation. Additionally, the solubilities of both the α-form and β-form were investigated in various solvents and mixed solvents. Recently, the selective crystallization of TTL polymorphs and solvates through antisolvent crystallization has been systematically studied.[17] The range and limits of polymorph existence, established based on theoretical background, were confirmed through experiments. This study was conducted at a high level of supersaturation ratios between 9.2 and 18.0, and antisolvent ratios between 0.78 and 0.85. The formation zones of each polymorph and solvate were mapped according to the supersaturation ratio and antisolvent ratio. To enable selective crystallization of TTL, factors such as nucleation rate, solubility ratio, and interfacial energy were also investigated.

In addition, evaporative crystallization, which is advantageous for large-scale production and the manufacturing of coarse particles, is recommended as the crystallization method.[18,19] However, the application of evaporative crystallization in polymorph control is very rare.[20–24] For example, it has been reported that evaporative crystallization was used to extensively form the desired solvate of carbamazepine.[24] Studies on polymorph or solvate control in evaporation mode have been required to compare with the cooling and antisolvent crystallization modes primarily applied to APIs. Therefore, this study aims to achieve this goal by applying the evaporative crystallization method to TTL production.

This study focuses on the selective formation of solvates and polymorph chosen for pharmaceutical use. The metastable TTL form was obtained through evaporative crystallization. The polymorphic/solvate characteristics of TTL were studied and explained using powerful analytical techniques that allow for the identification and control of polymorphic/solvate forms during the crystallization process. Offline polymorph/solvate analysis techniques include optical microscopy, powder X-ray diffraction (PXRD), differential scanning calorimetry (DSC), thermogravimetric analysis (TGA), Fourier-transform infrared spectroscopy (FTIR), and Raman spectroscopy.[25,26] The effects of factors such as evaporation rate, supersaturation level, solvent, temperature, and concentration on TTL polymorphism/solvation during the evaporative crystallization were investigated. The formation conditions of both hydrate and anhydrous forms were identified and compared both thermally and physically. Furthermore, an attempt was made to understand these factors and optimize the conditions for crystallization of polymorphs/solvates selectivity in order to optimize the control process. Additionally, the hydrate crystals of TTL, α-form and β-form, were compared with the anhydrous polymorph γ-form.

2 Experiment

2.1 Materials

Taltireline (TTL) was used after purification by cooling crystallization in water. The molecular formula of anhydrous TTL is $C_{17}H_{23}N_7O_5$, with a molecular weight of 405.41 and a mass fraction purity of 0.996 or higher. Methanol, ethanol, 1-propanol, and isopropanol were obtained from Aldrich as analytical reagent grade (mass fraction purity > 0.995). Re-distilled deionized water was used in the experiments.

2.2 Evaporative crystallization experiment

The experimental setup is shown in Fig. 1. This system consists of a double-jacketed crystallizer, mechanical stirrer, temperature-controlled bath, vacuum pump, and drying equipment. The experiments were conducted in a semi-batch mode. The crystallizer is a cylindrical glass vessel with a 500 mL jacket, and it is equipped with a 4 cm propeller-type stirrer. A known quantity of β-form TTL crystals was dissolved in an appropriate amount of water (solvent) at a temperature 10 °C higher than the saturation temperature for 30 minutes to ensure complete dissolution of the TTL. After dissolution, the TTL solution was adjusted to the operating temperature and maintained at this temperature. Once a transparent solution was obtained, evaporative crystallization was carried out at the fixed operating temperature, vacuum level, and stirring speed. The liquid level of the evaporated solvent was continuously monitored. The operating temperature was set between 30 °C and 60 °C, and the stirring speed was fixed at 300 rpm. The amount of evaporated water, temperature, and pressure were measured as a function of elapsed time. The evaporation rate was controlled by adjusting the vacuum pressure while maintaining the temperature as a variable. Experiments were conducted at temperatures ranging from 30 to 60 °C, with the pressure varied between 1 and 150 Torr. TTL crystals were sampled, filtered, and dried before being used for solvate analysis, solution concentration, and optical microscopy analysis. The solvent and solid concentrations at the nucleation

point, nucleation time, and experimental elapsed time were recorded to calculate the amount of evaporated solvent, solvent evaporation rate, and supersaturation. The solid was separated through vacuum filtration and dried in an oven at 40 °C for 24 hours. Raman spectroscopy analysis confirmed that there were no changes in the crystal form before and after filtration or drying. Furthermore, the solid sample stored in a sealed container remained without any transformation even after four weeks. The crystals were verified offline using Powder X-ray diffraction (PXRD) and Raman spectroscopy, and characterized through FT-IR, TGA and DSC.

2.3 Characterization

PXRD analysis of solid samples was performed using an X-ray diffractometer (Smart Lab, Rigaku Co., Tokyo, Japan) with Cu Kα1 radiation (45 kV, 200 mA) over a 0–45° range. 50 mg of TTL powder was placed in a glass holder, and the sample surface was gently smoothed with a spatula and glass plate to prevent particle alignment, then the sample weight was accurately measured. Additionally, polymorphs/solvates were analyzed using Raman spectroscopy, which was identified by specific Raman peaks from previous studies and can measure both slurry and solid crystals.[14–17] Differential scanning calorimetry (DSC) analysis of polymorphs/solvates was obtained using a thermal analyzer (DSC1/Mettler-Tolledo, Germany). The operating conditions in the sealed pan system were as follows: sample weight, 5 mg; heating rate, 10°C min; N2 gas flow rate, 30 mL min^{-1}. Thermogravimetric analysis (TGA) of solid forms was performed using TA Instruments (TGA 1600 LF, Mettler-Tolledo, Germany) under dry nitrogen from 0 °C to 600 °C, with a gas flow rate of 30 mL min^{-1} and a heating rate of 10 °C min^{-1}. The shape of the polymorphs was observed using an optical microscope (Olympus CX31). Fourier-transform infrared spectroscopy (FT-IR) analysis of TTL was performed using a Nicolet 6700 (Thermo) with a DTGS KBr detector, KBr beam splitter, a wavelength range of 400–4000 cm^{-1}, and an Ever-Glo IR source.

2.4 Solubility

The solubility of α-form, β-form, and γ-form TTL in water was measured using the isothermal method.[16] The TTL and solvent mixtures were thoroughly mixed at a speed of 300 rpm and constant temperature. Solute was continuously added until no further particles dissolved. The temperature was controlled using a thermostatic bath ranging from 0 to 50 °C. Some experiments were repeated three times to confirm reproducibility, and the solubility at a given temperature was reproduced within 0.001 g of solute per 100 g of solution. The solubility experiments showed an error range of 0.001–0.003 kg kg^{-1} based on reproducibility tests of selected experiments, and the data in Fig. 6 are presented as average values. Therefore, the accuracy was approximately 99.70–99.90%.

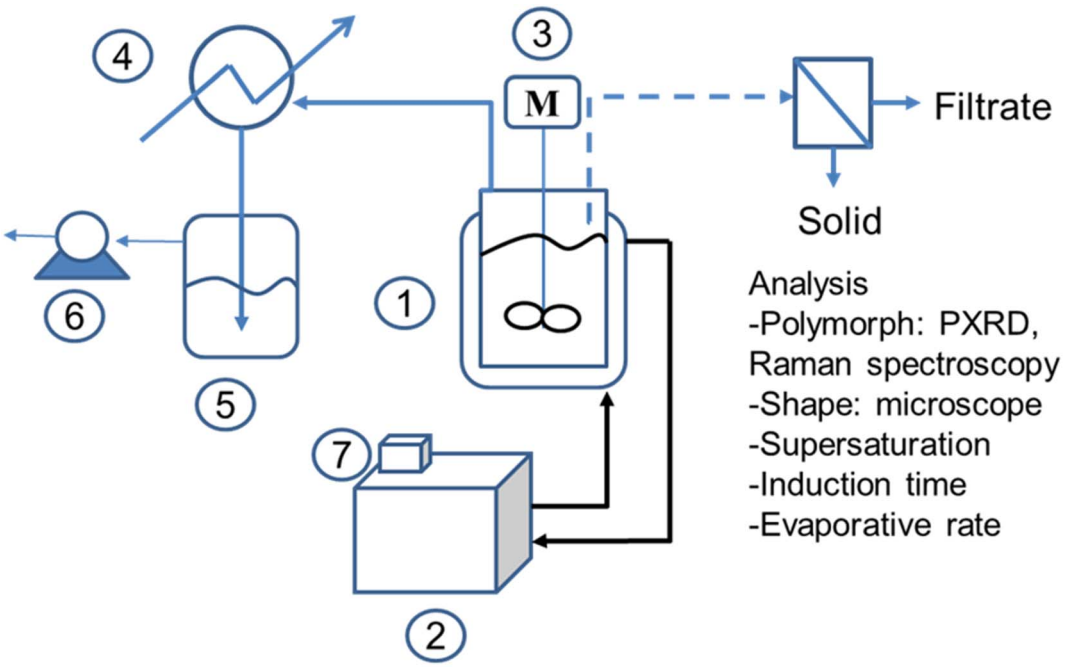

Fig. 1 Schematic diagram for evaporation experiment apparatus.

Table 1 Experimental data for evaporative crystallization in water

Run	Solvent	C_0 (kg kg^{-1})	Stirring (rpm)	Induction time (min)	Evaporation rate (m^3 s^{-1} m^{-2})	C_{met} (kg kg^{-1})	T (K)	C^* (kg kg^{-1})	S (−)	Form
E-1	Water	1.135	300	580	2.552×10^{-8}	7.309	318	1.992	3.670	α
E-2	Water	1.009	300	660	2.335×10^{-8}	6.709	318	1.992	3.368	α
E-3	Water	0.890	300	595	2.460×10^{-8}	9.454	318	1.992	4.747	α
E-4	Water	0.845	300	685	2.295×10^{-8}	6.526	318	1.992	3.277	α
E-5	Water	1.991	300	820	1.938×10^{-8}	14.658	318	1.992	7.359	α
E-6	Water	1.043	300	1260	1.278×10^{-8}	7.256	318	1.992	3.643	α
E-7	Water	1.128	300	1395	1.247×10^{-8}	11.093	318	1.992	5.570	α
E-8	Water	1.391	300	2805	1.392×10^{-8}	5.532	318	1.992	2.777	α
E-9	Water	1.107	300	1440	2.383×10^{-8}	5.803	318	1.992	2.914	α
E-10	Water	1.271	300	3315	1.567×10^{-8}	5.344	318	1.992	2.683	α
E-11	Water	0.665	300	3080	1.347×10^{-8}	5.428	318	1.992	2.725	α
E-12	Water	1.162	300	660	2.417×10^{-8}	8.542	318	1.992	4.289	α
E-13	Water	0.482	300	1430	1.317×10^{-8}	5.571	318	1.992	2.797	α
E-14	Water	1.624	300	1360	1.510×10^{-8}	5.687	318	1.992	2.855	α
E-15	Water	0.489	300	895	2.018×10^{-8}	4.496	313	1.196	3.760	α
E-16	Water	0.776	300	790	2.162×10^{-8}	6.476	313	1.196	5.416	α
E-17	Water	1.194	300	360	3.320×10^{-8}	5.297	313	1.196	4.430	α
E-18	Water	0.913	300	1150	1.420×10^{-8}	5.516	308	0.896	6.157	α
E-19	Water	0.596	300	680	1.443×10^{-8}	3.646	303	0.597	6.111	α
E-20	Water	0.446	300	480	3.328×10^{-8}	5.266	303	0.597	8.825	α
E-21	Water	0.702	300	4200	0.687×10^{-8}	1.601	313	1.196	1.339	β
E-22	Water	0.718	300	3450	0.612×10^{-8}	1.292	308	0.896	1.442	β
E-23	Water	0.845	300	3480	0.753×10^{-8}	1.506	308	0.896	1.681	β
E-24	Water	0.661	300	2560	0.847×10^{-8}	2.234	313	1.196	1.868	α + β
E-25	Water	0.760	300	2360	1.188×10^{-8}	2.614	308	0.896	2.918	α + β
E-26	Water	0.833	300	2060	0.960×10^{-8}	2.165	308	0.896	2.416	α + β
E-27	Water	0.895	300	2590	1.148×10^{-8}	3.360	308	0.896	3.750	α + β
E-28	Water	0.280	300	2550	0.733×10^{-8}	1.205	303	0.597	2.019	α + β

3 Results and discussion

3.1 Evaporation rate and polymorphs of TTL

Evaporative crystallization experiments for the production of α-form and β-form TTL were conducted using water as the solvent. The solution temperature was controlled and set by the temperature controller. The operating temperatures were set at 30 °C, 35 °C, 40 °C, 45 °C, and 60 °C. At 60 °C, the solubility increased sharply, and the solution became very viscous, with the surface easily gelating. In this case, it was difficult to stir the

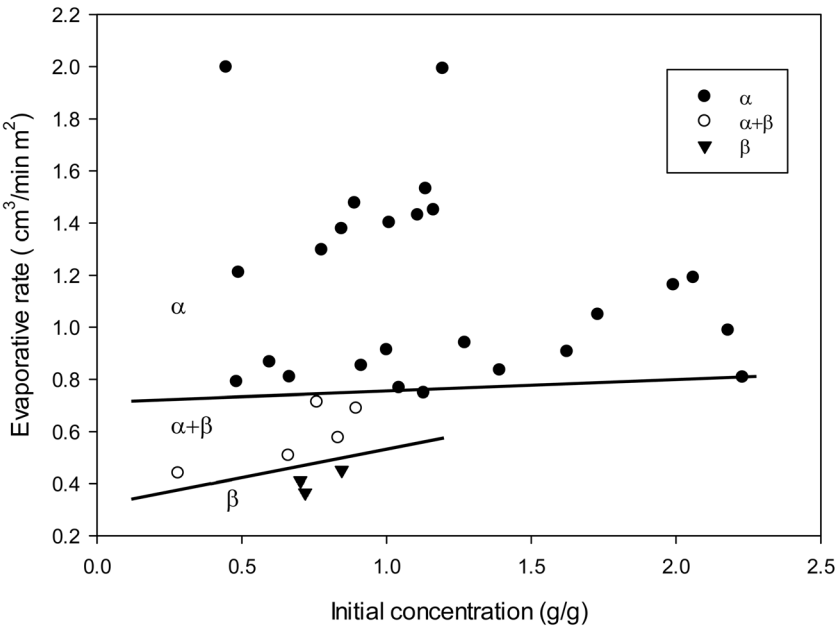

Fig. 2 Evaporation rate and polymorphs of TTL.

Table 2 Evaporative experiments in alcohol

Run	Solvent	C_0 (kg kg^{-1})	Stirring (rpm)	Evaporation rate (m^3 s^{-1} m^{-2})	C_{met} (kg kg^{-1})	T (K)	Induction time (min)	C^* (kg kg^{-1})	S (−)	Form
Et-1	Ethanol	0.3755	300	1.16×10^{-7}	0.4524	323	240	0.3953	1.1446	γ
Et-2	Ethanol	0.7372	300	3.00×10^{-7}	0.9331	343	210	0.7760	1.2025	γ
Et-3	Ethanol	0.3048	300	3.17×10^{-8}	0.3586	318	510	0.3208	1.1176	γ
Me-1	Methanol	0.5323	300	1.90×10^{-7}	0.6571	328	240	0.5603	1.1728	γ
Me-2	Methanol	0.5122	300	1.03×10^{-7}	0.6567	328	210	0.5392	1.2179	γ
1P-1	1-Propanol	0.2347	300	4.79×10^{-6}	0.3352	323	15	0.2470	1.3571	γ
1P-2	1-Propanol	0.3109	300	1.59×10^{-5}	0.5014	343	5	0.3272	1.5323	γ
1P-3	1-Propanol	0.3109	300	2.45×10^{-6}	0.4201	343	30	0.3272	1.2838	γ
IPA-1	IPA	0.1159	300	3.33×10^{-6}	0.1525	323	15	0.1220	1.2500	γ
IPA-2	IPA	0.1618	300	6.97×10^{-6}	0.2247	343	10	0.1703	1.3194	γ
IPA-3	IPA	0.1618	300	2.30×10^{-6}	0.1997	343	30	0.1703	1.1728	γ

solution. Despite the very high evaporation rate, no crystals formed after a long time of experimentation at this temperature. The weight of the evaporated solution was measured before and after the experiment and at the point of nucleation, determining the amount of evaporated solvent, induction period, evaporation rate, and supersaturation. The details of the evaporative crystallization experiments in water are provided in Table 1 and Fig. 2. In Fig. 2, the solvate (hydrate) formation region is shown with respect to initial concentration and evaporation rate. This plot is very scattered and unrelated. It seems that the solvate selection is simply determined by the magnitude of the evaporation rate. At the lowest evaporation rate of 0.412 cm^3 (min·m^2)$^{-1}$ or below, only the β-form was formed, whereas a mixture of α-form and β-form was obtained at evaporation rates between 0.440 and 0.713 cm^3 (min·m^2)$^{-1}$. At higher evaporation rates of 0.748 to 1.991 cm^3 (min·m^2)$^{-1}$, the experimental results showed that the α-form crystals were completely formed. Evaporative crystallization experiments for the production of γ-form TTL were conducted using alcohol solvents. The conditions and results for this experiment are presented in Table 2. Crystals formed at various alcohol solvents and evaporation rates were analyzed. In alcohol solvents, only the γ-form was obtained at evaporation rates ranging from 1.9 to 954.0 cm^3 min^{-1}·m^{-2}, indicating that this form is an anhydrous crystal form. The effect of evaporation rate on TTL polymorphs is presented as a representative example in Fig. 3 through PXRD pattern. The coexistence of the α- and β-forms was qualitatively confirmed by the blue PXRD pattern. Quantitative phase analysis was not performed because the PXRD data were used in an offset form for phase identification. Accordingly, the PXRD patterns are discussed in terms of qualitative polymorph identification rather than quantitative phase fractions.

3.2 Effect of evaporation rate on supersaturation

Evaporation rate is a key variable in evaporative crystallization as it significantly influences supersaturation.[27,28] The

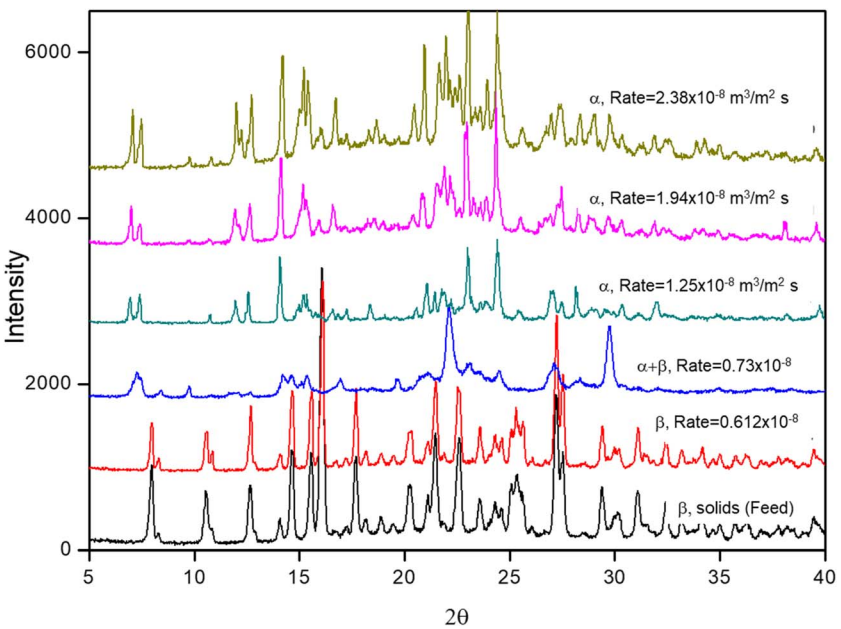

Fig. 3 PXRD patterns of samples prepared at different evaporation rates, α, β and α + β forms.

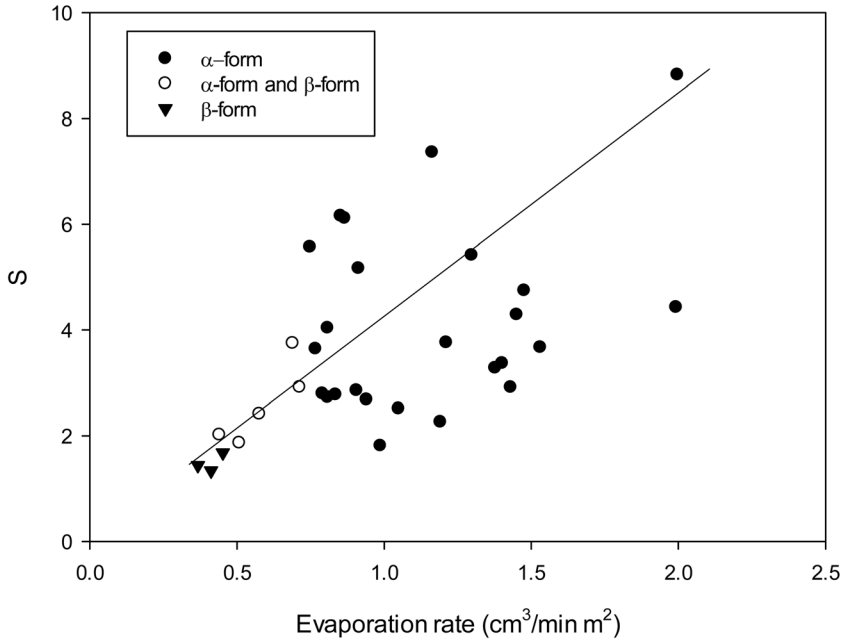

Fig. 4 Effect of evaporative crystallization on supersaturation.

experimental results of this study were analyzed using operating variables such as temperature, initial concentration, evaporation time, and amount of evaporation. The conditions under which the α-form, β-form, and their mixtures are formed were identified under all the experimental settings investigated. Fig. 4 illustrates the effect of evaporation rate on supersaturation. Although the data a highly scattered, what is due to differences in concentration, solubility, and temperature. Overall, it was observed that supersaturation increases with increasing evaporation rate. The regions where the β-form, α-form, and their mixtures are formed were identified.

As shown in Fig. 4 and Table 1, the nature of the nucleating polymorph depends on the supersaturation (S) of the solution. The β-form can be obtained at low supersaturation, while a mixture of α-form and β-form occurs within the supersaturation range of 1.81 to 3.73. In both cases, the equilibrium concentration ranges between 0.6 g g^{-1} and 1.2 g g^{-1}. Conversely, at a higher equilibrium concentration of 1.992 g g^{-1} (*i.e.*, when the operating temperature is 45 °C), all samples formed the α-form, with a supersaturation range from 2.7 to 7.4. In cases where the saturation concentration is relatively low, ranging from 0.597 to 1.196 (*i.e.*, when the operating

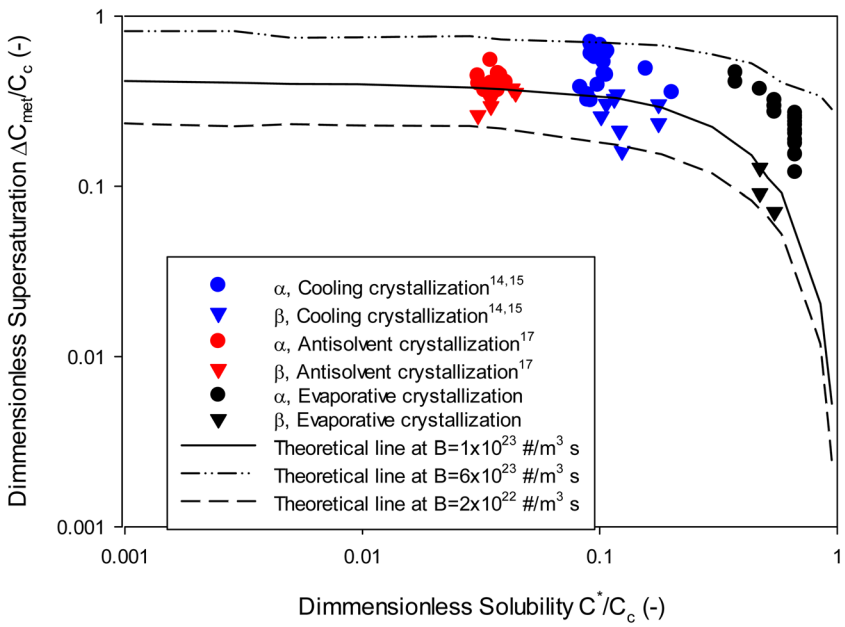

Fig. 5 The relationship between dimensionless supersaturation and dimensionless solubility, for all experimental data.

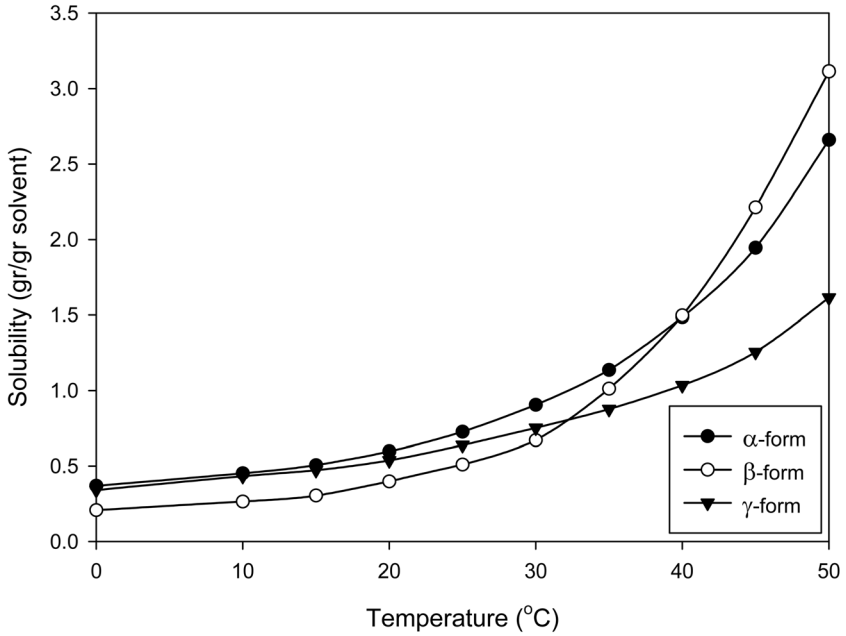

Fig. 6 Solubility of γ-form with the comparison with α-form and β-form, all measured in water as a solvent.

temperature is 30–40 °C), it was observed that the α-form is only formed within a supersaturation range of 3.8 to 8.8. Solutions that generated high supersaturation exhibited a tendency to form the α-form, which is a metastable polymorph under those conditions. In contrast, the β-form or mixtures of α-form and β-form were obtained at lower supersaturations. Similar results have been reported at crystallization of polymorphs of famotidine and clopidogrel.[29,30] These two APIs exhibit both metastable and stable polymorphs. At low supersaturation (S), the stable polymorph nucleates, whereas at high supersaturation, the metastable polymorph nucleates.

3.3 Relationship between supersaturation and solubility at polymorphic/solvated nucleation

The rate of heterogeneous nucleation is expressed as the following equation[19,31–33]

$$B_{\text{het}} = 0.965\varphi_{\text{het}} D_{\text{AB}} (N_{\text{A}} C_{\text{c}})^{\frac{5}{3}} \left(\frac{C^*}{C_{\text{c}}}\right)^{7/3} S^{7/3} \sqrt{f \ \ln \ C_{\text{c}}/C^*} \exp\Big[-1.19 \ (\ln \ C_{\text{c}}/C^*)^3 (\ln \ S)^{-2}\Big]$$

and $S = \dfrac{C}{C^*}$

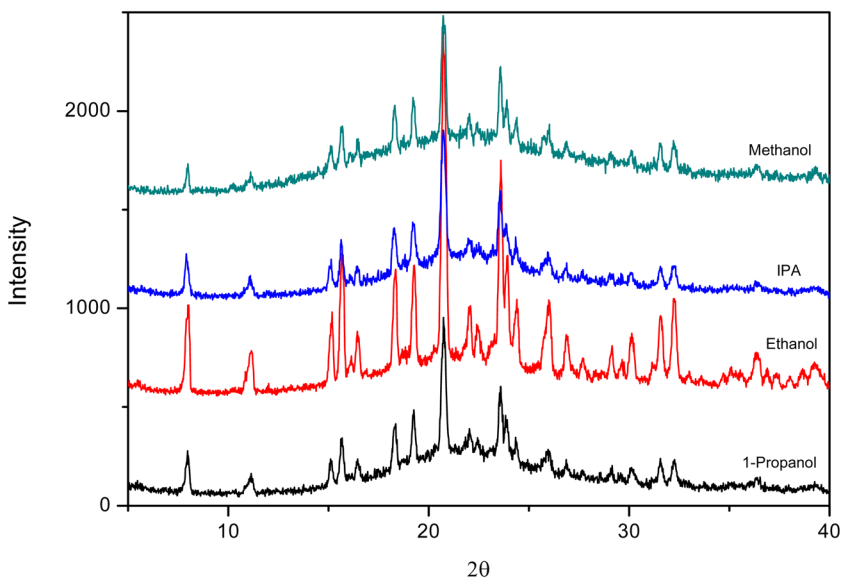

Fig. 7 PXRD patterns of γ-form which carried out in different alcohol solvents.

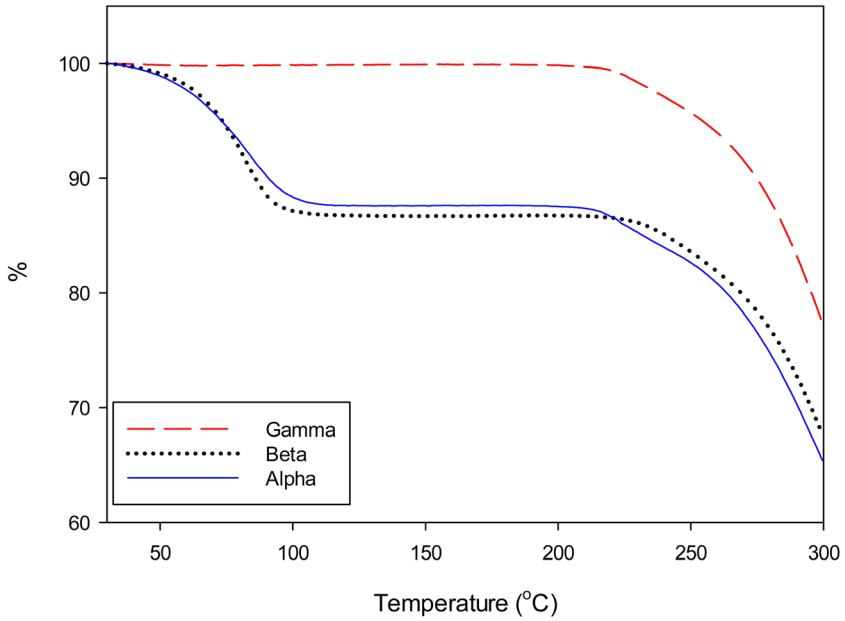

Fig. 8 TGA thermograms of 3 forms of TTL.

where φ_{het}, D_{AB}, N_A, C_c, C^* and C are heterogeneity factor, diffusion coefficient, Avogadro number, crystal molar density, solubility and concentration, respectively.

The supersaturation obtained from evaporative crystallization were compared with the polymorphic formation conditions previously reported for cooling crystallization[14] and antisolvent crystallization.[17] Fig. 5 shows the relationship between dimensionless supersaturation and dimensionless solubility, including all experimental data. The three crystallization methods exhibit different behaviors within the solubility range. The dimensionless solubility ranges for evaporative, cooling, and antisolvent crystallizations are 0.35 to 0.70, 0.081 to 0.2, and 0.027 to 0.046, respectively.

In crystallization, the nucleation rate of polymorphs/solvates can be compared based on the relationship between dimensionless supersaturation and dimensionless solubility. Mersmann *et al.*[19,31] derived a theoretical relationship between the metastable zone width, ΔC_{met}, and solubility, C^*, for various nucleation processes. In their model, the dimensionless metastable zone width, $\Delta C_{met}/C_c$, is plotted against the dimensionless solubility, C^*/C_c, for a constant nucleation rate. This method was used to determine the nucleation rate of polymorphs/solvates.

The diffusion coefficient, D_{AB}, for TTL in water and organic solvents is approximately 1.59×10^{-9} m^2 s^{-1}.[17] The three nucleation rate curves shown in Fig. 5 are appropriately applied for $D_{AB} = 1.59 \times 10^{-9}$ m^2 s^{-1}, $C_c = 3.1$ kmol m^{-3}, $?_{sus} = 10^{-12}$, and $f = 0.1$. These theoretical plots were compared with all the data obtained from the three crystallization methods. In the plots shown in Fig. 5, the nucleation rate curve positions higher as B_{het} increases.

The solubility of TTL in the investigated solvents ranges from 0.0868 to 2.325 kmol m^{-3}, resulting in a dimensionless solubility range of C^*/C_c from 0.028 to 0.750 (where $C_c = 3.1$ kmol m^{-3}). For heterogeneous nucleation, the plot of $\Delta C_{met}/C_c$ against C^*/C_c determines the nucleation zones for polymorph formation based on nucleation rate. According to this study, the α-form is obtained when $1 \times 10^{23} < B_{het} < 6 \times 10^{23}$ nuclei per m^3 s, whereas the β-form is obtained when $2 \times 10^{22} < B_{het} < 1 \times 10^{23}$ nuclei per m^3 s. Thus, this plotting method provides critical insights into nucleation rates for selective polymorph/solvate formation and can also be applied to predict new polymorphs/solvates.

3.4 Achieving anhydrous TTL by evaporation in alcohol solvents

In this study, the presence of the anhydrous form was confirmed using TGA (removal of hydration water), DSC (thermal events), XRD (crystallinity and phase identification), and IR (hydrate/anhydrate difference). Combining thermal analysis (TGA/DSC) and structural analysis (PXRD, Raman spectroscopy, FTIR) can provide information on new polymorphs, solvates, and amorphous solids.[25,26] In the evaporative crystallization experiment using alcohol as the solvent, the anhydrous form, γ-form of TTL was obtained. The TTL form obtained from the alcohol solvents investigated in this study all appeared as the same anhydrous form. Characterization of the γ-form was performed, and the results are presented below.

3.4.1 Solubility of TTL polymorphs/solvates in water. The solubility of the γ-form was investigated from 0 to 50 °C. The solubility curve of the γ-form is shown in Fig. 6 and compared with the solubility curves of the α-form and β-form, which were presented previously. The γ-form exhibits lower solubility than the α-form at all temperatures but shows higher solubility than the β-form between 0 °C and 32 °C. However, above 32 °C, the β-form exhibits higher solubility than the γ-form. This figure

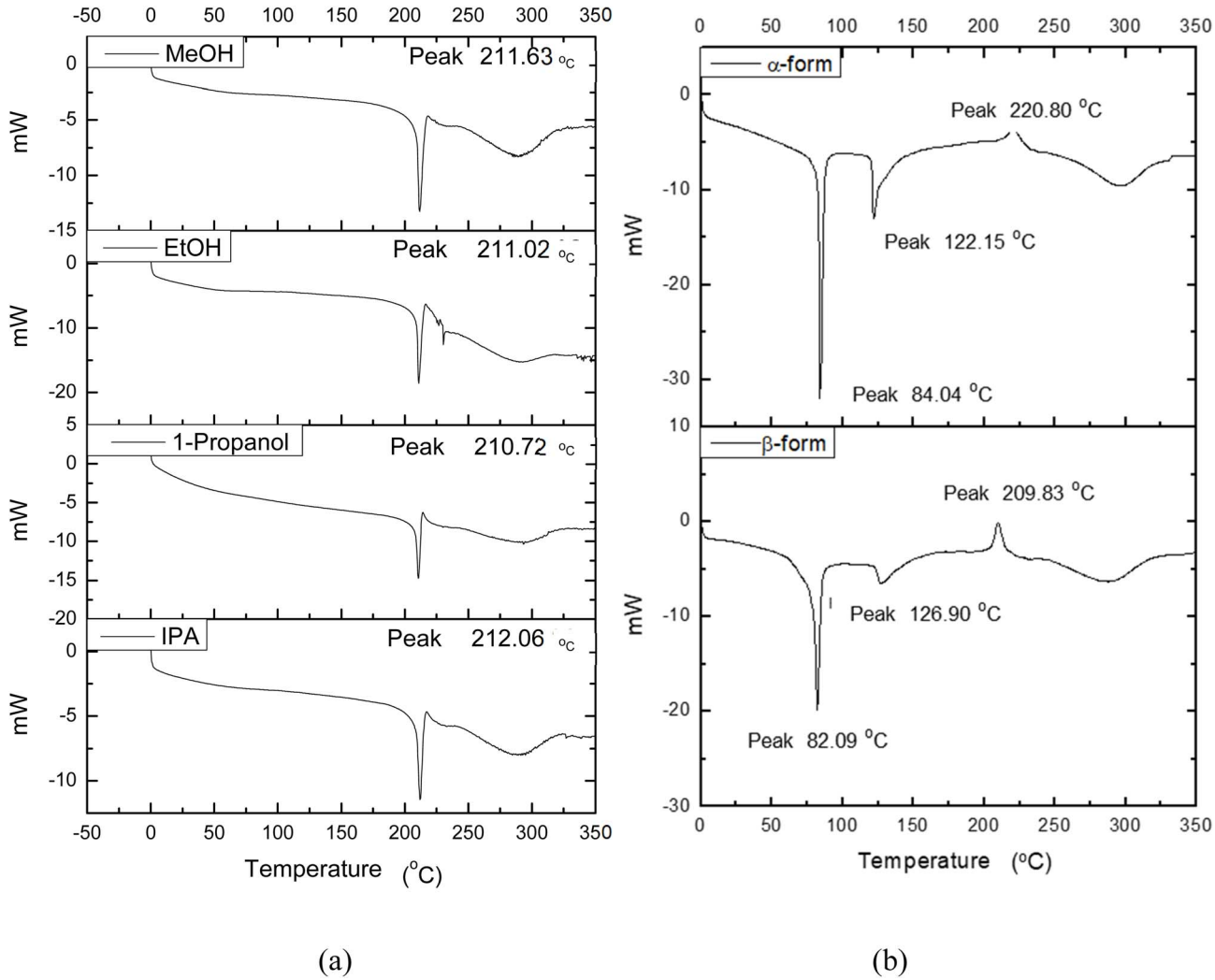

Fig. 9 DSC curves of anhydrous γ-form in different solvents (a) and DCS curves of hydrate forms (b).

illustrates the intersection of the solubility curves of the three forms at two specific temperatures. The transition point between the solubility curves of the α-form and β-form is 40 °C, while the solubility curves of the β-form and γ-form intersect at approximately 33 °C. No intersection points were observed between the solubility curves of the α-form and γ-form within the investigated temperature range. This figure represents an enantiotropic system, indicating reversible transitions between polymorphs at specific transition temperatures.

3.4.2 PXRD patterns for crystallization in water and alcohols. When compared to the PXRD patterns of the hydrated α- and β-forms, the PXRD pattern of the γ-form is entirely distinct (see Fig. SI2). As mentioned earlier, the γ-form was obtained through evaporation in alcohol solvents. Four alcohol solvents, methanol, ethanol, 1-propanol, and isopropanol (IPA), were used. The PXRD patterns of the γ-form obtained from different alcohol solvents are presented in Fig. 7. The TTL polymorphs obtained from alcohol solvents all appeared in only one form.

3.4.3 TGA/DSC analysis. Fig. 8 shows TGA thermal analysis curves of TTL. TGA distinguishes hydrates from anhydrates because hydrates show characteristic mass loss from dehydration, whereas anhydrates exhibit no such weight loss. In the TGA thermal analysis curve of the γ-form, weight loss is observed only once, whereas, as mentioned earlier, the α- and β-forms show two major weight losses. The first weight loss occurs at temperatures below 100 °C, which indicates the loss of water from the structure. However, this phenomenon was not observed in the γ-form. This suggests that the α- and β-forms are hydrates, while the γ-form is an anhydrous form. All three forms show a significant weight loss around 212 °C, which indicates the decomposition of TTL. The hydrates show a water loss of approximately 14%, and the calculated result corresponds to about 3.7 hydrates, *i.e.*, the tetrahydrate (TTL·$4H_2O$). DSC analysis of a 5 mg TTL hydrate sample at a heating rate of 10 °C min^{-1} showed a clear endothermic dehydration peak between 80 and 140 °C. The integrated peak area was approximately −965.8 mW °C, corresponding to a total enthalpy of about −5.79 J. This equals −474.5 kJ mol^{-1} on a molar basis. Given that TGA confirmed a 14% water loss, the dehydration enthalpy per mole of water was estimated to be −149 kJ mol^{-1}. Overall, TTL hydrate exhibits a distinct endothermic dehydration process upon heating.

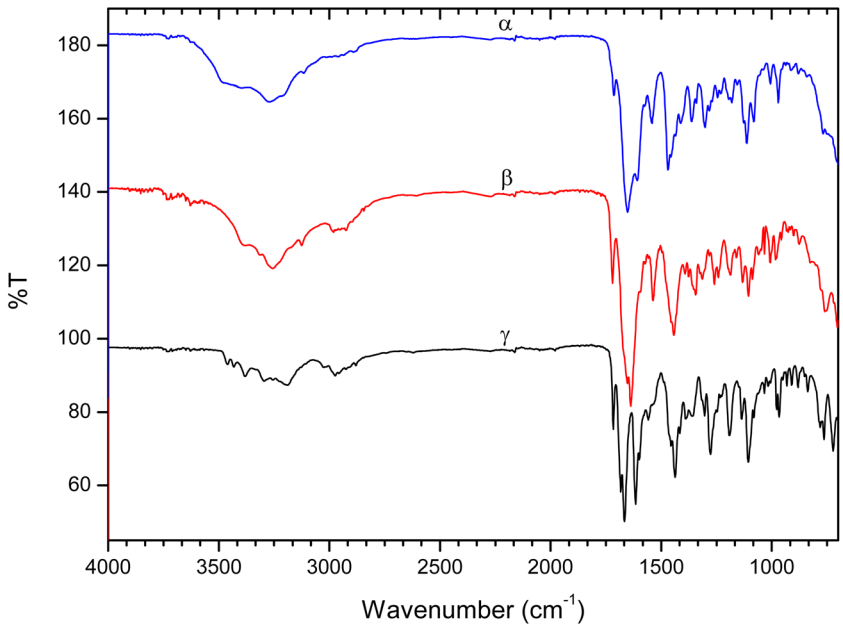

Fig. 10 FT-IR spectra of 3 forms of TTL.

DSC distinguishes hydrates from anhydrates because hydrates exhibit endothermic dehydration peaks, whereas anhydrates lack these events and show only their intrinsic melting or transition behavior. Fig. 9 shows the DSC thermal analysis curves of the γ-form (a) and the α- and β-forms (b) in different solvents. The DSC curve of the γ-form exhibits an endothermic peak around 211 °C, while the DSC curves of the α- and β-forms show endothermic peaks at 84.04 °C and 122.15 °C, and 82.09 °C and 126.9 °C, respectively.

3.4.4 IR analysis. The IR spectrum of the γ-form is presented in Fig. 10, followed by the IR spectra of the α- and β-forms. The three peaks observed around 3500 cm^{-1} are characteristic of the γ-form and are not seen in the α- and β-forms. The absorption peak at 3630 cm^{-1} is characteristic of the β-form and is not observed in the α-form. The absorption at 1718 cm^{-1}, based on the C=O stretching vibration, is weak in the α-form but appears as a distinct and strong peak in the β-form. The hydrate exhibits an H–O–H bending peak near 1630 cm^{-1}, whereas the anhydrate does not show this peak, which supports that the γ-form is an anhydrous form.

3.4.5 Others. PXRD patterns, Raman patterns and microscopic photos of α, β and γ are shown in Fig. SI2–SI4, respectively. From the comparison of these tools, distinct differences among the three polymorphs/solvates can be observed. Eventually, clear differences in the PXRD patterns of α,β and γ-forms can be observed in Fig. 3 and 7. In addition, unambiguous identification can also be achieved using DSC, TGA, IR, and Raman analyses.

4 Conclusions

This study focused on the selective formation of solvates or polymorphs of TTL through evaporative crystallization. The effects of evaporation rate, supersaturation, solvent type, temperature, and concentration on the solvation/polymorphism of TTL during evaporative crystallization were investigated. The formation conditions of the hydrated and anhydrous crystals were identified, and their thermal and physical properties were comparatively analyzed. Additionally, these factors were studied to optimize the solvate control process and investigate the conditions for selective crystallization of polymorphs. While the α-form and β-form are hydrated crystals of TTL, the γ-form, an anhydrous crystal with entirely different characteristics from the hydrated forms, was also comparatively analyzed.

To control the selection of α- and β-forms of TTL crystals, the effect of evaporation rate was considered. At evaporation rates of 0.412 $cm^3\ (min \cdot m^2)^{-1}$ or below, only the β-form was formed, whereas a mixture of the α-form and β-form was obtained at evaporation rates of 0.440–0.713 $cm^3\ (min \cdot m^2)^{-1}$. At relatively high evaporation rates of 0.748–1.992 $cm^3\ (min \cdot m^2)^{-1}$, the α-form crystals were formed. In evaporative crystallization, the evaporation rate influenced the supersaturation, and the selective nucleation of crystals primarily depended on the supersaturation (S) of the solution. The β-form was obtained at $S < 1.68$, while a mixture of the α-form and β-form appeared in the range of $1.86 < S < 3.75$. In both cases, the solubility ranges from 0.6 to 1.2 g g^{-1}. Conversely, when the solubility was 1.992 g g^{-1} (*i.e.*, at an operating temperature of 45 °C), all samples formed the α-form, with supersaturation in the range of 2.7–7.4. Solutions with higher supersaturation tended to form the α-form, which is a metastable form. On the other hand, the β-form or a mixture of the α- and β-forms could be obtained at lower supersaturation. Regardless of the supersaturation during evaporative crystallization, the γ-form was obtained from methanol, ethanol, 1-propanol, and isopropanol (IPA) solvents.

The crystallization characteristics of TTL solvates were studied and described using analytical techniques capable of identifying and controlling polymorphic/solvated forms during the crystallization process. Offline analysis techniques included optical microscopy, powder X-ray diffraction (PXRD), differential scanning calorimetry (DSC), thermogravimetric analysis (TGA), Fourier-transform infrared spectroscopy (FTIR), and Raman spectroscopy. These analyses successfully distinguished the hydrated forms α and β, and the anhydrous form γ. Solubility measurements in water revealed that the β-form is stable below 34 °C, while the γ-form is stable above 34 °C.

The supersaturation conditions obtained from evaporative crystallization were compared with the previously reported polymorph/solvate formation conditions of cooling crystallization and antisolvent crystallization. The three crystallization methods exhibited different operational solubility ranges. The dimensionless solubility ranges were 0.35 to 0.70 for evaporative crystallization, 0.081 to 0.2 for cooling crystallization, and 0.027 to 0.046 for antisolvent crystallization. The nucleation rates of polymorphs/solvates in crystallization could be calculated and compared using plots of dimensionless supersaturation against dimensionless solubility. According to this study, the α-form was obtained when the nucleation rate was in the range of $1 \times 10^{23} < B_{het} < 6 \times 10^{23}$ nuclei per m^3 s, while the β-form was obtained when $2 \times 10^{22} < B_{het} < 1 \times 10^{23}$ nuclei per m^3 s. Thus, this approach provides critical information on nucleation rates for selective polymorph/solvate formation and can also be applied to predict new polymorphs/solvates.

Conflicts of interest

There no conflicts to declare.

Symbols

B_{het}	Nucleation rate, $m^3\ s^{-1}$
C_c	Crystal molar density, g g^{-1}, kmol m^{-3}
C	Concentration, g g^{-1}, kmol m^{-3}
D_{AB}	Diffusion coefficient, $m^2\ s^{-1}$
f	Heterogeneous nucleation factor
N_A	Avogadro number, $kmol^{-1}$
S	Relative supersaturation, –

Data availability

The data supporting this article are available from the corresponding author. Supplementary information (SI) is available. See DOI: https://doi.org/10.1039/d5ra07845h.

Acknowledgements

This study was conducted under a collaborative research agreement on crystallization technology between Verfahrenstechnik/TVT (Martin-Luther-University Halle-Wittenberg) and Crystallization Research Center (Hanbat National University) since 2004.

References

1 H. G. Brittain, *Polymorphism in Pharmaceutical Solids*, Marcel Dekker, 1999.
2 B. Bechtloff, S. Nordhoff and J. Ulrich, *Cryst. Res. Technol.*, 2001, **36**, 1315–1328.
3 J. Guo, M. J. Jones and J. Ulrich, *Chem. Eng. Res. Des.*, 2010, **88**, 1648–1652.
4 J. Ulrich and M. J. Jones, *Chem. Eng. Res. Des.*, 2004, **82**, 1567–1570.
5 J. Kim and J. Ulrich, *Cryst. Res. Technol.*, 2022, **57**, 2100176.
6 J. Kim and J. Ulrich, *Ind. Eng. Chem. Res.*, 2022, **61**, 7052–7066.
7 M. Kitamura, *Cryst. Growth Des.*, 2004, **4**, 1153–1159.
8 A. L. Linas and J. M. Goodman, *Drug Discov Today*, 2008, **13**, 198–210.
9 J. Ulrich and C. Strege, *J. Cryst. Growth*, 2002, **237**, 2130–2135.
10 J. Ulrich, *Chem. Eng. Technol.*, 2003, **26**, 832–835.
11 S. Maruyama, H. Ooshima and J. Kato, *Chem. Eng. J.*, 1999, **75**, 193–200.
12 S. Maruyama and H. Ooshima, *J. Cryst. Growth*, 2000, **212**, 239–245.
13 S. Maruyama and H. Ooshima, *Chem. Eng. J.*, 2001, **81**, 1–7.
14 L. T. N. Dang and K. J. Kim, *Chem. Eng. Technol.*, 2015, **38**, 1059–1067.
15 L. T. N. Dang and K. J. Kim, *Chem. Eng. Technol.*, 2016, **39**, 1281–1288.
16 L. T. N. Dang, K. J. Kim and J. of, *Chem. Eng. Japan*, 2018, **51**(3), 216–221.
17 L. T. N. Dang, J. Kim, K. J. Kim and J. Ulrich, *Chem. Eng. Technol.*, 2025, **48**(10), e70111.
18 J. W. Mullin, *Crystallization*, Elsevier Science, 2001.
19 A. Mersmann, *Crystallization Technology Handbook*, Taylor & Francis, 2001.
20 S. Hellstén, B. Han, E. Mäkilä, H. Niemi, J. Salonen, V. P. Lehto, T. Stelzer, M. Louhi-Kultanen and J. Ulrich, *Chem. Eng. Technol.*, 2013, **36**, 1300–1306.
21 N. Tohnai and S. Ito, *Chem.–Eur. J.*, 2018, **24**, 4343–4349.
22 F. T. H. Qu, M. Louhi-Kultanen and J. Rantanen, *J. Cryst. Growth*, 2009, **311**, 2580–2589.
23 F. Tian, H. Qu, M. Louhi-Kultanen and J. Rantanen, *Chem. Eng. Technol.*, 2010, **33**, 833–838.
24 H. Desai, L. Rao and P. Amin, *Am. J. Pharm. Tech. Res.*, 2014, **4**, 479–493.
25 J. Kim and J. Ulrich, *Chem. Eng. Technol.*, 2022, **45**, 291–301.
26 J. Kim and J. Ulrich, *Ind. Eng. Chem. Res.*, 2022, **61**, 14609–14625.
27 K. M. Jim, K. J. Kim and Y. N. Jang, *Ind. Eng. Chem. Res.*, 2013, **52**, 11151–11158.
28 J. J. Lu and J. Ulrich, *Cryst. Res. and Technol.*, 2005, **40**, 839–846.
29 K. M. Jim and K. J. Kim, *Chem. Eng. Technol.*, 2012, **35**, 995–1002.
30 J. Lu, X. J. Wang, X. Yang and C.-B. Ching, *J. Pharm. Sci.*, 2007, **96**, 2457–2468.
31 A. Mersmann, *Chem. Eng. Res. Des.*, 1996, **74**, 812–820.
32 K. J. Kim and A. Mersmann, *Chem. Eng. Sci.*, 2001, **56**, 2315–2323.
33 K. J. Kim and M. F. Doherty, *AIChE*, 2015, **61**, 1372–1379.